Invariant Manifolds near L_1 and L_2 in the Sun-Jupiter Elliptic Restricted Three-Body Problem I.*

Gladston Duarte[(1)], Àngel Jorba[(2,3)]

September 19, 2023

(1) Dipartimento di Ingegneria Meccanica e Aerospaziale, Politecnico di Torino, Via Duca degli Abruzzi 24, 10129, Torino, Italy.

(2) Departament de Matemàtiques i Informàtica, Universitat de Barcelona, Gran Via de les Corts Catalanes 585, 08007 Barcelona, Spain.

(3) Centre de Recerca Matemàtica, Edifici C, Campus Bellaterra, 08193 Bellaterra, Spain

E-mails: <gladston.duarte@polito.it>, <angel@maia.ub.es>.

Abstract

In this paper, we present a way of combine the computation of invariant tori and their stable and unstable manifolds with the multiple shooting technique. We start by showing some of the results of [Jor01] that should be modified in order to introduce the multiple shooting technique in these computations. After that it is introduced, by a direct application in the Planar Elliptic Restricted Three-Body Problem (PERTBP), how to modify the equations and methods to compute the above-mentioned objects. It is shown, in particular, the structure of the (systems of) equations and matrices involved in these computations. An application of these computations can be found in [DJ23a], where the dynamics of comet 39P/Oterma is modelled as a PERTBP.

Keywords: Computation of tori; Computation of invariant manifolds; multiple shooting; Planar Elliptic Restricted Three-Body Problem; Lagrangian points.

*This work has been supported by the Spanish grant PID2021-125535NB-I00 (MCIU/AEI/FEDER, UE) and the catalan grant 2021 SGR 01072. G.D. acknowledges the support from the Spanish Ministry of Economy and Competitiveness through the "María de Maeztu" Programme for Units of Excellence in R&D (MDM-0445-2014) and the support of Polish National Science Centre grant 2018/29/B/ST1/00109.

Contents

1 Introduction

The dynamics of comet 39P/Oterma is known to experience a fast transition between heliocentric orbits inside and outside of the orbit of Jupiter ([HB98]). It is remarkable that, during this transition, the comet passes close to the Lagrangian points L_1 and L_2 of the Sun-Jupiter system.

The simplest model to study this transition is the well-known Planar Circular Restricted Three-body Problem (PCRTBP). The PCRTBP describes the motion of an infinitesimal particle (the comet) under the combined gravitational attraction of two primaries (Sun and Jupiter), which are assumed to move in circular orbits around their common centre of mass. Besides, the particle is assumed to move in the plane defined by the motion of the primaries. It is common to use a rotating system of reference (usually called synodical reference frame) so that the origin is at the centre of mass and Sun and Jupiter are kept fixed on the x axis. The unit of length is the Sun-Jupiter distance, the unit of mass is the total mass of the system and the unit of time is that the gravitational constant is equal to one. With these units, the period of Jupiter is 2π. Calling μ to the mass of Jupiter, the Sun is located at $(\mu, 0)$ and Jupiter is at $(-1+\mu, 0)$. Is is also well-known that this model has five equilibrium points [Sze67], three of them ($L_{1,2,3}$, or collinear points) on the x axis and two of them ($L_{4,5}$ or triangular points) defined as the third vertex of the equilateral triangle that has the primaries as the other two vertices (see Figure 1).

The collinear points are of centre×saddle type, so they are unstable. The well known Lyapunov centre theorem [MO17] implies the existence of a one-parametric family of periodic orbits that are born at the equilibrium point. This family is also unstable and, near the point, each periodic orbit in the family has a stable and a unstable manifold. It is remarkable that the manifolds of these periodic orbits meet so that there is a intricate network of connections between the neighbourhoods of L_1 and L_2 [KLMR00, GKL$^+$04, CM06, CDMR06].

The transition of Oterma has been studied, using the PCRTBP, in [KLMR01] where it has been shown that the invariant manifolds of the Lyapunov orbits near L_1 and L_2 can be used to connect orbits outside that of Jupiter with orbits inside, and vice versa. In [DJ23b] explicit normal form calculations around $L_{1,2}$ are used to identify the concrete periodic orbits and their manifolds that organise this transition.

In this paper we focus on a periodic time-dependent perturbation of the PCRTBP, the Planar Elliptic Restricted Three-Body Problem (PERTBP). In this model, Jupiter moves not in a circular but on an elliptic orbit. The phenomenon of the transition experimented by Oterma is caused by heteroclinic connections between objects (Lyapunov periodic orbits in the case of the PCRTBP, and the equivalent ones, in the PERTBP) around L_1 and L_2. Another important application of this study of heteroclinic connections is the computation of a chain for fast Arnold diffusion in the PERTBP [CD23].

1.1 Description of the model

The Planar Elliptic Restricted Three Body Problem, PERTBP, models the motion of an infinitesimal particle under the gravitational attraction of two massive bodies that move on elliptical orbits around their common centre of mass. As before, by infinitesimal we mean that the particle is attracted by the two massive bodies but its mass is so small that its effect on the bodies can be neglected. In what follows we will focus on the Sun-Jupiter case.

There are several systems of coordinates which are common to use for this model. The one that is used in this paper is also known as roto-pulsating and it is inspired by the synodical system of

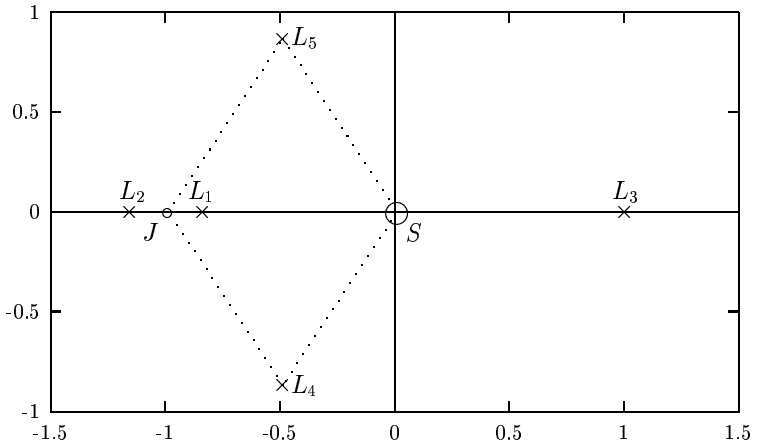

Figure 1: The positions of the equilibrium points in the Sun-Jupiter RTBP.

coordinates of the PCRTBP. The origin is taken as the centre of mass, and the x axis is defined as the line joining Sun and Jupiter, so it rotates with a non-constant angular velocity. The unit of length is taken in a time-dependent way, so it expands and contracts periodically in time (creating an effect of pulsation) such that Sun and Jupiter have fixed coordinates on this axis and their relative distance is always 1. The positive direction on the x line is from Jupiter to the Sun. The z axis is parallel to the angular momentum of the system and the y-axis is chosen to obtain a positive-oriented system of coordinates. The plane $z = 0$ is invariant by the motion of the particle and, as the motion of Oterma takes place very close to this plane, we restrict ourselves to $z = 0$. It is usual to take units of time and mass such that the period of Sun and Jupiter is 2π, and the total mass of the system is 1. With these units, the gravitational constant is also equal to 1. Calling μ to the mass of Jupiter, the Sun is located at $(\mu, 0)$ and Jupiter is at $(-1 + \mu, 0)$.

To write the equations of motion in a simple way it is common to use the true anomaly instead of time (see [Sze67] for details). Then, the Hamiltonian for this problem is non-autonomous and can be written in the following way,

$$H(x, y, p_x, p_y, f) = \frac{1}{2}\left((p_x + y)^2 + (p_y - x)^2\right) - \frac{1}{1 + e\cos f}\left(\frac{1}{2}(x^2 + y^2) + \frac{1-\mu}{r_1} + \frac{\mu}{r_2}\right), \qquad (1)$$

where $r_1^2 = (x-\mu)^2+y^2$, $r_2^2 = (x+1-\mu)^2+y^2$ and e is Jupiter's eccentricity and f is its true anomaly that here plays the role of the time. The parameter values used here are $\mu = 0.0009538811803631$ and $e = 0.04859403602748$.

1.2 Goal

We will focus on the neighbourhood of L_1 and L_2 of the PERTBP. If the eccentricity e is zero, is the classical PCRTBP and these points are of centre×saddle type, with a one-parametric family of periodic orbits emanating from them. If e is non zero but small enough, these families of periodic orbits become (Cantorian) families of 2D tori, see [JV97b]. These tori have two basic frequencies: one is the frequency of a periodic Lyapunov orbit while the second one is the perturbing frequency, 1 in this case. Moreover, as the equilibrium point has a saddle direction, these tori have stable and unstable manifolds that organise the arriving/departing trajectories. Our primary goal is to show,

for the Sun-Jupiter case, how these manifolds serve as a bridge that connects the neighbourhoods of L_1 and L_2 between them and with outside regions, in a similar manner as it happens on the PCRTBP. In a following paper [DJ23a] we will show that the PERTBP provides a much better description of the transition of Oterma (because the position of Jupiter is very important when passing nearby). In [DJ23a] we have identified which tori and manifolds guide the motion of Oterma during this transition and we have use them to have an accurate description of its motion. The computation of these heteroclinic connections between different tori also allow for the computation of a chain for the Arnold diffusion in the PERTBP. In [CD23] the authors use the data produced in this work to compute an initial guess and estimates for a real orbit diffusing in this model, using connections of tori from different frequencies around L_1.

1.3 Summary of the paper

Section 2 explains the numerical methods used to compute the Lyapunov families of 2D tori around $L_{1,2}$. It is common to use a Poincaré section to reduce the dimensionality of the problem and, specially, the dimension of the torus that becomes a 1D invariant curve. In periodically forced ODEs it is common to use the temporal section given by the period of the flow (this is sometimes called an stroboscopic map), which results in an autonomous discrete dynamical system. We stress that this is not an option in this case, since the unstability of the regions around $L_{1,2}$ is so high that most of the initial conditions near these points are sent far away after 2π units of time, which makes the stroboscopic map useless to study the dynamics near $L_{1,2}$. A standard tool to deal with this situation is to use multiple shooting techniques. In Section 2 we explain a multiple shooting method to compute invariant tori, including the computation of their linear stability. The main difference with previous works ([Jor01]) is that the computation of the Floquet change and the reduced matrix has to be adapted to a multiple shooting environment. In Section 3 we discuss how we have adapted a method for the computation of invariant manifolds to multiple shooting, and Section 4 shows some of the obtained tori, their invariant manifolds and how they provide a network connecting regions outside the orbit of Jupiter with regions inside and viceversa.

2 Numerical approximation of invariant tori

A standard first step to compute invariant objects of flows is to apply a suitable Poincaré section so that the dimension of the invariant object is reduced by one. In this way, the computation of periodic orbits becomes the computation of fixed points, and the computation of 2D tori becomes the computation of 1D invariant curves. The case of very unstable periodic orbits can be very difficult since the error growth during the numerical integration needed to return to the section can be so big that the accurate computation of the periodic orbit becomes very difficult or impossible. To solve this difficulty, it is common to use a multiple shooting method [SB02]. Here we combine the multiple shooting method used to find periodic orbits with a method to compute invariant 2D tori (for a version of these methods adapted to parallel computers see [GJNO22]). Next we will summarise a method to compute invariant tori and next we will explain how it is modified to be used in combination with multiple shooting.

2.1 Single shooting

As the PERTBP is a 2π-periodic perturbation of the RTBP, the Lyapunov periodic orbits around L_1 and L_2 with frequencies that are non resonant with the frequency 1 become 2D tori if the eccentricity is small enough. The method we use to compute them is a modification of the method in [CJ00]. To explain it, let us start by considering the (stroboscopic) section $f = 0 \pmod{2\pi}$. This is a 4D autonomous map P. Then, the 2D tori of the flow become 1D invariant curves of P, with a frequency ω that comes from the frequency of a periodic orbit of the RTBP. This is, if $\varphi : \mathbb{T}^1 \to \mathbb{R}^4$ is a parametrization of the invariant curve, it satisfies,

$$P(\varphi(\theta)) = \varphi(\theta + \omega), \quad \forall \theta \in \mathbb{T}^1, \tag{2}$$

which can be written in the form of a functional equation,

$$F(\varphi, \omega)(\theta) = P(\varphi(\theta)) - T_\omega(\varphi)(\theta) = 0, \quad \forall \theta \in \mathbb{T}^1, \tag{3}$$

where T_ω is the linear operator defined by $T_\omega(\varphi)(\theta) = \varphi(\theta + \omega)$. The option considered here is to solve this equation by means of a Newton method. Let us first discuss the case in which ω is known which, as we will see, it is the case here. It is natural to approximate φ by a truncated Fourier series,

$$\varphi(\theta) \approx \varphi_N(\theta) = a_0 + \sum_{k=1}^{N} a_k \cos(k\theta) + b_k \sin(k\theta), \qquad a_0, a_k, b_k \in \mathbb{R}^4, \quad \forall k = 1, \ldots, N.$$

The chosen value for N has to do with the accuracy of the approximation of the curve, and its value will be discussed later on in this section. For now, let us choose some fixed value for it. The idea is to solve a discretized version of equation (3) on the mesh $\theta_j = 2\pi j/(2N+1)$, $j = 0, \ldots, 2N$. Then, given a truncated Fourier series $\varphi_N^{(0)}$, we can evaluate it to produce a table of values for $F(\varphi_N^{(0)}, \omega)$,

$$F_j = P\left(\varphi_N^{(0)}\left(\frac{2\pi j}{2N+1}\right)\right) - \varphi_N^{(0)}\left(\frac{2\pi j}{2N+1} + \omega\right), \quad j = 0, \ldots, 2N.$$

To apply a Newton method, we can compute the derivatives of the values F_j w.r.t. the coefficients a_k, b_k of $\varphi_N^{(0)}$ by means of the chain rule, as discussed in [CJ00, Jor01]. Let us note that the number of unknowns (a_k, b_k) and the number of equations coincides. Let us also note that, as the Poincaré map P is autonomous, the representation of an invariant curve is not unique: if $\varphi(\theta)$, $\theta \in \mathbb{T}^1$, is a representation of an invariant curve, for any $\beta \in \mathbb{T}$, $\varphi(\theta + \beta)$ is another representation of the same curve (i.e., the Fourier coefficients of $\varphi(\theta)$ and $\varphi(\theta + \beta)$ are different). This implies that equation (2) has a 1D manifold of solutions. This is usually solved by adding an extra condition, typically to ask that some coordinate has a prescribed value when $\theta = 0$ [CJ00, GJ04]. This implies that the linear system to be solved at each step of the Newton method has one extra condition, which is solved using Gaussian elimination with pivoting (the pivoting sends a linearly dependent equation to the last row, which is then ignored since it has to be linearly dependent of the previous ones).

2.1.1 Error estimates

After succesfully computing, via a Newton's method, a set of Fourier coefficients such that $\|F_j\|$ is small enough for all j, we should check if they represent an invariant curve of the Poincaré map P

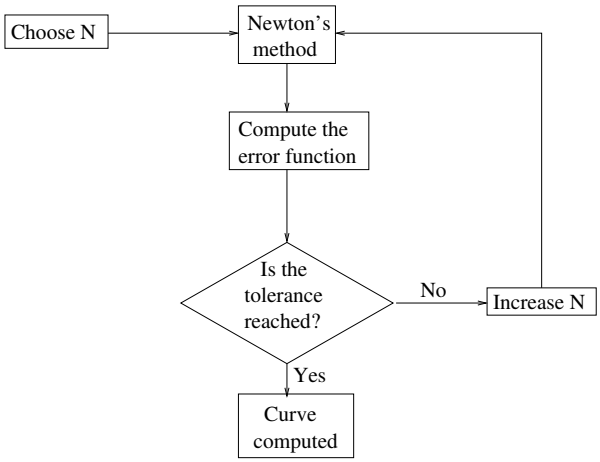

Figure 2: Algorithm for the determination of N.

within a certain level of accuracy. To this end, for a given ω, we use

$$E(\varphi) = \max_{\theta \in \mathbb{T}^1} \|F(\varphi)(\theta)\|,$$

that we estimate by using a much finer mesh (typically, with 10 or 100 times more points) than the one used for the discretization. If this value is greater than the required level of accuracy, it means that a larger number of Fourier modes (i.e., a larger N) is needed. Therefore, N is increased and the computation is restarted using the previous invariant curve as starting point, see Figure 2,

2.1.2 Initial conditions for the Newton method

As it has been mentioned before, the frequencies of the Lyapunov tori near $L_{1,2}$ are the ones of Lyapunov orbits of the RTBP plus the perturbing frequency of the PERTBP, which is exactly 1. To compute these tori we have computed first the family of Lyapunov periodic orbits when the eccenctricity e is zero and we consider the time-2π flow for this case $e = 0$. A Lyapunov periodic orbit with irrational frequency ω_0 is then seen as an invariant curve for the time-2π map when $e = 0$: if the periodic orbit is parametrized from 0 to 2π, then a point on the orbit advances $\omega = 2\pi\omega_0$, which is the frequency of the curve. We have used this invariant curve as the starting point of a continuation method w.r.t. e, till the eccentricity of Jupiter is reached. Note that in all the continuation process the frequency of the invariant curve is known and constant. More details are given in Section 2.4.

2.2 Multiple shooting

Due to the high instability of the region near $L_{1,2}$ we will combine the methods summarised in Section 2.1 with a multiple shooting technique [SB02]. To this end, we will use four temporal sections for the angular variable f, $f_j = \frac{j}{4}2\pi$, $j = 1, \ldots, 4$. We denote each of these sections by Σ_{f_j}, the codimension 1 manifold defined as

$$\Sigma_{f_j} = \{(x, y, p_x, p_y, f) \in \mathbb{R}^4 \times \mathbb{T}^1 \text{ such that } f = f_j\}.$$

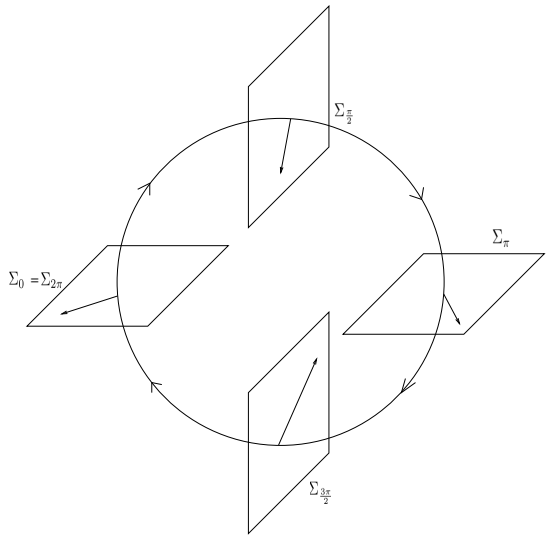

Figure 3: Illustration of the multiple shooting used for the PERTBP.

Let us denote by P^j, $j = 0, \ldots, 3$, the flow between sections Σ_{f_j} and $\Sigma_{f_{j+1}}$. Therefore, the time-2π flow of the PERTBP, starting at $f = 0$, is given by $P = P^3 \circ P^2 \circ P^1 \circ P^0$, see Figure 3. In this context, to look for an invariant torus is to look for four curves, φ_j, $j = 0, 1, 2, 3$ (one for each section), such that

$$\begin{cases} P^0(\varphi_0(\theta)) = \varphi_1(\theta), \\ P^1(\varphi_1(\theta)) = \varphi_2(\theta), \\ P^2(\varphi_2(\theta)) = \varphi_3(\theta), \\ P^3(\varphi_3(\theta)) = T_\omega(\varphi_0(\theta)). \end{cases} \tag{4}$$

Each of these curves φ_j is approximated by a truncated Fourier series and, similarly as before, their coefficients are found by considering the equations

$$\begin{cases} F^0(\varphi)(\theta) = P^0(\varphi_0(\theta)) - \varphi_1(\theta), \\ F^1(\varphi)(\theta) = P^1(\varphi_1(\theta)) - \varphi_2(\theta), \\ F^2(\varphi)(\theta) = P^2(\varphi_2(\theta)) - \varphi_3(\theta), \\ F^3(\varphi)(\theta) = P^3(\varphi_3(\theta)) - T_\omega(\varphi_0(\theta)). \end{cases} \tag{5}$$

where we are using the notation $\varphi = (\varphi_0, \varphi_1, \varphi_2, \varphi_3)$. As usual, these equations are discretized by representing the curves φ_j as a truncated Fourier series,

$$\varphi_j(\theta) = a_{0,j} + \sum_{k=1}^{N} a_{k,j} \cos(k\theta) + b_{k,j} \sin(k\theta),$$

and the system is solved iteratively by means of a Newton method. The computation of the Jacobian is similar to the single shooting case, taking into account that not all the equations depend on all

the unknowns (the coefficients $a_{k,j}$, $b_{k,j}$). This implies that the Jacobian has the form

$$\begin{pmatrix} \left.\frac{\partial F^0}{\partial c_0}\right|_\theta & \left.\frac{\partial F^0}{\partial c_1}\right|_\theta & 0 & 0 \\ 0 & \left.\frac{\partial F^1}{\partial c_1}\right|_\theta & \left.\frac{\partial F^1}{\partial c_2}\right|_\theta & 0 \\ 0 & 0 & \left.\frac{\partial F^2}{\partial c_2}\right|_\theta & \left.\frac{\partial F^2}{\partial c_3}\right|_\theta \\ \left.\frac{\partial F^3}{\partial c_0}\right|_{\theta+\omega} & 0 & 0 & \left.\frac{\partial F^3}{\partial c_3}\right|_\theta \end{pmatrix},$$

where c_i represent the coefficients a_{0i}, a_{ji}, b_{ji}.

2.2.1 Initial conditions

We have already mentioned before (Section 2.1.2) that the invariant tori near $L_{1,2}$ can be found by means of a continuation method starting from the Lyapunov periodic orbits that exists for the RTBP (that is, PERTBP for $e = 0$), increasing the eccentricity till its value for the Sun-Jupiter system. If we are using multiple shooting, initial conditions have to be given for each curve φ_j, $j = 0, \ldots, 3$. Let us see how we obtain them.

Given a Lyapunov periodic orbit (for $e = 0$), we start by computing four different parameterizations for this orbit, each one with a time shift of $\pi/2$ units of time,[1] that is, the time needed to go from one section to the next. In this way, the periodic orbit is seen as four invariant curves φ_j, $j = 0, \ldots, 3$ that solve (5) when $\omega = 2\pi\omega_p$, being ω_p the frequency of the periodic orbit. These curves are the starting point of the continuation process till the Sun-Jupiter eccentricity is reached.

2.3 Linear stability

The linear stability of an invariant curve φ of a discrete dynamical system $\bar{x} = P(x)$, $x \in \mathbb{R}^n$, is given by the linear skew product

$$\begin{cases} \overline{x} = A(\theta)x, \\ \overline{\theta} = \theta + \omega, \end{cases} \tag{6}$$

where $A(\theta) = D_x P(\varphi(\theta))$. This sytem is called reducible when there exists a change of variables $y = C(\theta)x$, continuous with respect to θ, such that the above system can be written as

$$\begin{cases} \overline{y} = By, \\ \overline{\theta} = \theta + \omega, \end{cases} \tag{7}$$

where $B = C^{-1}(\theta+\omega)A(\theta)C(\theta)$ does not depend on θ (and it is usually called the reduced matrix). The dynamics of system (7) can be easily studied by computing the eigenvalues of B.

It is known ([Jor01]) that, if a skew product (6) is reducible, the matrix B and the change of variables C can be obtained by studying the following generalized eigenvalue problem: find the couples (λ, ψ) such that

$$A(\theta)\psi(\theta) = \lambda T_\omega \psi(\theta), \tag{8}$$

[1] To simplify the language, we refer to the true anomaly f as the time of the PERTBP.

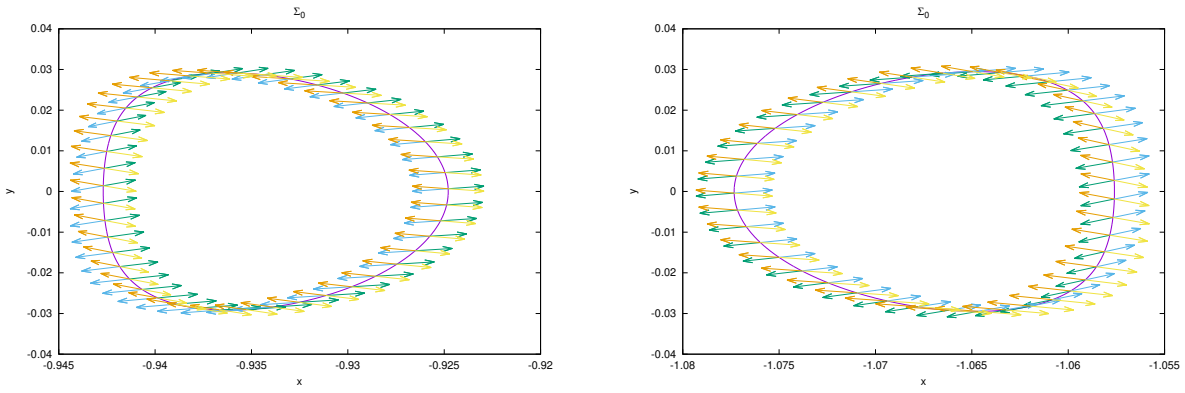

Figure 4: Invariant curves around L_1 (left) and L_2 (right) in the section $f = 0$. The arrows are vectors that are tangento to the stable and unstable manifolds at each point of the invariant curve.

where $\lambda \in \mathbb{C}$ and ψ belongs to the space of continuous functions from $\mathbb{T}^1$ to $\mathbb{R}^n$ endowed with the sup norm. We note that, as this is a eigenproblem in an infinite dimensional space, the set of eigenvalues can be empty, or to contain infinitely many values. In this case, the eigenvalues are organised in circles.

To compute these eigenvalues, we rewrite (6) as

$$T_{-\omega} \circ A(\theta)\psi(\theta) = \lambda\psi(\theta) \tag{9}$$

and we discretize the operator $T_{-\omega} \circ A$ using truncated Fourier series. This allows to compute a finite set of eigenvalues/eigenvectors and to choose the right ones, $\{(\lambda_i, \psi_i)\}_{i=1}^n$ so that the reduced matrix B is $\mathrm{diag}(\lambda_1, \ldots, \lambda_n)$ and $C = (\psi_1, \ldots, \psi_n)$, see [Jor01] for more details.

If an eigenvalue, say λ_1, is real and different from ± 1 the eigenfunction is the linear approximation to the corresponding invariant manifold. That is, the linear approximation to the invariant curve φ is given by

$$(\theta, \tau) \mapsto \varphi(\theta) + \tau\psi_1(\theta),$$

which is tangent to the invariant manifold at $\tau = 0$. This is illustrated in Figure 4.

2.3.1 Multiple shooting

Let us see how to adapt the previous methods to compute the linear stability of an invariant curve to a multiple shooting environment. We focus on the case where four sections have been used, but the methods can be easily adapted to any number of sections.

Let us denote by φ_j the curve contained in section Σ_{f_j}, $j = 0, \ldots, 3$ such that (4) holds, and let us define $A^i(\theta) = D_x P^i(\varphi_i(\theta))$. If we consider φ_0 as the invariant curve for the map $P^3 \circ P^2 \circ P^1 \circ P^0$ then its linear stability follows from the eigenproblem $A^3 \cdot A^2 \cdot A^1 \cdot A^0\, u = \lambda\, T_\omega\, u$ which, due to the high instability of the curve, involves huge numbers and it is not suitable for numerical computations.

Therefore, to avoid the product of these matrices we consider the following eigenproblem,

$$\begin{cases} A^0 u = \sigma v, \\ A^1 v = \sigma w, \\ A^2 w = \sigma z, \\ \hat{A}^3 z = \sigma u, \end{cases} \Leftrightarrow \begin{pmatrix} & & & \hat{A}^3 \\ A^0 & & & \\ & A^1 & & \\ & & A^2 & \end{pmatrix} \begin{pmatrix} u \\ v \\ w \\ z \end{pmatrix} = \sigma \begin{pmatrix} u \\ v \\ w \\ z \end{pmatrix}, \tag{10}$$

where $\hat{A}^3 = T_{-\omega} \cdot A^3$. It is easy to see that the eigenvalues σ of this problem are the 4th roots of the eigenproblem that corresponds to single shooting, that is, $A^3 \cdot A^2 \cdot A^1 \cdot A^0 \, u = \sigma^4 \, T_\omega \, u$.

As before, we discretize this problem by using truncated Fourier series. As it happens for single shooting, it is necessary to choose the right set of eigenvalues/eigenfunctions to have an accurate reresentation of the reducing change of variables and the reduced matrix ([Jor01]). Figure 4 shows a plot of the stable/unstable directions of φ_0.

2.4 Continuation

The computation of families of invariant tori usually starts with the computation of a first torus in the family followed by a continuation to obtain the family in the interested range. When dealing with a Lyapunov family, sometimes the initial torus is computed near the fixed point of the map where the family is born, using information from the linear dynamics around the point [CJ00, GM01, GJ04]. Here we have used a different approach, as explained in Section 2.1.2: we have computed a periodic orbit for $e = 0$ and we have continued it with respect to e till the eccentricity of Jupiter. Next, we have kept e constant and we have used the frequency of the invariant curve as the continuation parameter to compute the Lyapunov family of invariant curves.

The families of invariant curves are not continuous, they have a "small hole" around each resonance. If the system is analytic, the size of these holes decreases exponentially with the order of the resonance [JV97a] so that the family has a Cantor structure. The set of holes in the family has small measure. Due to this Cantor structure, the continuation of a family of invariant curves can be tricky sometimes. If we are in a zone where all resonances are of high order, the holes are so small that are below the resolution of the double precision arithmetic of the computer so that the family looks continuous. On the other hand, near a low order resonance we expect to have a larger hole that can break the continuation process if we try to look for a torus inside. The standard solution for this difficulty is to choose a larger continuation step so that the next tori we try to compute is "at the other side" of the hole. For this reason, it is common to compute first the family with a low accuracy and with a continuation stepsize that is not too small. These results can be used later as initial points for a more accurate computation.

In this case, we have used a continuation step in the frequency of 10^{-4} and an accuracy in the approximation of the invariant curve of 10^{-9}. They are quite small but the continuation has succeded with these values. Once the family has been computed, it would be easy to increase the accuracy of some of these tori if needed: adding a suitable number of Fourier modes, a single step of the Newton process will be enough to match the level of accuracy of the numerical integrator of the ODE ([JZ05]).

Figure 5 shows some of the computed tori around L_1 and L_2.

With the above specification of the continuation parameter, the continuation step and the tolerance value, we have computed 7270 invariant curves around L_1, with rotation number $\omega \in$

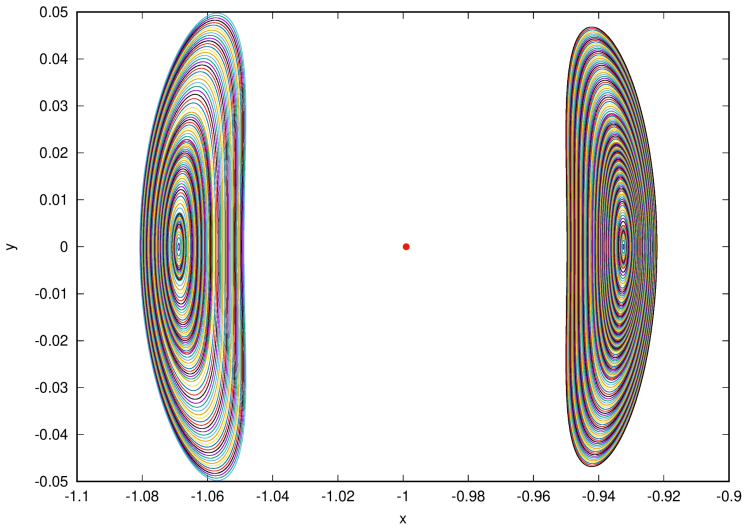

Figure 5: Illustration of the parallel shooting used in this work for the PERTBP: 4 sections in the independent variable.

$[0.394274086132195, 1.121174086130501]$, and 4498 invariant curves around L_2, with rotation number $\omega \in [5.694237631679274, 6.143937631678226]$. These invariant curves correspond to 2D tori for the flow, with two basic frequencies: one of them is always 1 and come from the eccentricity of Jupiter while the other is $\omega/(2\pi)$, being ω the rotation number of the corresponding invariant curve. This means that the second frequency is in the range $[2.06275066974, 2.17844039787]$ (L_1) and $[1.90626606621, 1.97783804413]$ (L_2).

For these tori, the eigenvalues related to the unstable direction are on the range $[3.60319538152 \times 10^6, 2.08973695728 \times 10^7]$ (L_1) and $[7.33764362520 \times 10^5, 2.64109300607 \times 10^6]$ (L_2), which means that, in the worst case, the instability will be related to the maximum 4th root of these values, which is given by 67.61186347293.

The continuation has stopped at some distance from $L_{1,2}$, enough to study the dynamics of comet Oterma ([DJ23a]), which is the main motivation for these computations. This number of computed tori was also used in [CD23] for the computation of a chain of Arnold diffusion.

3 Computation of the stable and unstable manifolds of a torus

The Lyapunov invariant tori near $L_{1,2}$ have a stable and an unstable invariant manifold. As it has been discussed in Section 2.3, the linear approximation to these manifolds is given by the corresponding eigenfunctions of the eigenproblem (8). To produce a global approximation to these manifolds we follow the ideas in [Sim90]. To simplify the presentation, let us focus first in the case of an unstable manifold, so let $\lambda \in \mathbb{R}$, $\lambda > 1$ (this is what happens near $L_{1,2}$ so we do not discuss the case $\lambda < -1$) the unstable eigenvalue and ψ its eigenfunction, so that the linear approximation to the unstable manifold can be parametrized as in (9). A fundamental set of an invariant manifold is a piece of the manifold that spans the full manifold by the iteration (backward and forward) of the Poincaré map. Here, a fundamental set is given by the cylinder

$$(\theta, \tau) \in \mathbb{T} \times [h_0,\, h_0\lambda] \mapsto \varphi(\theta) + \tau\psi_1(\theta).$$

If $|h_0|$ is chosen small enough, this cylinder is close to the true manifold (at a distance of $O_2(h_0)$) and it can be used to span the whole manifold by simply applying the dynamics to a suitable mesh of points on the cylinder. We note that both values $\pm h_0$ have to be used to generate both "sides" of the manifold.

Let us now see how the ideas of fundamental domain and multiple shooting can be combined to produce a satisfactory visualization of the invariant stable/unstable manifolds in the case of a highly-unstable environment. In this case, let us call σ the unstable eigenvalue of (10), and $(\psi_0, \ldots, \psi_3)$ the eigenfunction (we recall that σ^4 is an eigenvalue of (8), the eigenproblem for the single shooting case). The linear approximation to the invariant manifolds is given by

$$(\theta, \tau) \mapsto \{(\varphi_j(\theta) + \tau\psi_j(\theta))\}_{j=0}^{3}\,. \tag{11}$$

Note that, in this case, the dynamics is as follows:

$$\begin{aligned} &P^j(\varphi_j(\theta) + \tau\psi_j(\theta)) = \varphi_{j+1}(\theta) + \tau\sigma\psi_{j+1}(\theta) + O_2(\tau), \qquad j = 0, 1, 2, \\ &P^3(\varphi_3(\theta) + \tau\psi_3(\theta)) = \varphi_0(\theta + \omega) + \tau\sigma\psi_0(\theta + \omega) + O_2(\tau). \end{aligned} \tag{12}$$

As it has been commented before, we will use the linear approximation to produce an approximation to a fundamental cylinder, $(\theta, \tau) \in \mathbb{T} \times [h_0, \sigma h_0]$. To this end, we have chosen the value $|h_0| = 10^{-5}$. Then, we use a mesh of equispaced values in θ and τ on the fundamental domain, we use (11) to produce a mesh on the manifold and we apply the dynamics to grow the manifold.

As $|h_0|$ is small, several iterates are needed to move away from the invariant curve. On the other hand note that, near the torus, the initial error in the approximation of the manifold does not grow when we apply the dynamics, since the remaining directions are attracting (the stable direction) or neutral (the directions of the family of tori). The error only starts to increase when we move away from the manifold.

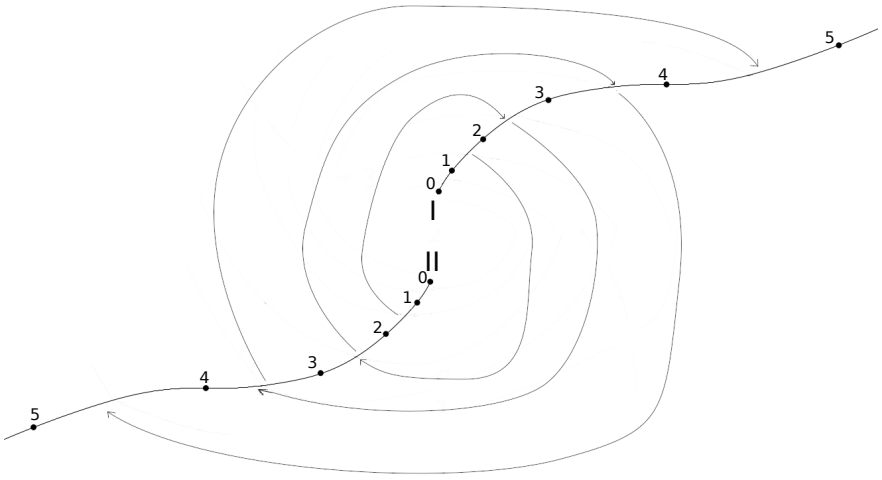

Figure 6: Illustration on how the parallel shooting technique can be used together with the fundamental domain concept in order to have a more precise computation of the invariant manifolds of a torus, using only 2 sections for simplicity. I and II represent the sections and the numbers from 0 to 5 points in these sections. See text for full details.

Figure 6 shows, schematically, the computation of the invariant manifolds in a multiple shooting situation, in the case of two sections, namely I and II. Let $Q^0 : I \to II$ and $Q^1 : II \to I$ the mapping from one section to the other one given by the flow. The points labeled with the number 0 represent the tori, so there is one on each section. The continuous curves starting at point 0 represent their manifolds. The numbers along the curve (from 1 to 5) denote points on the manifolds. Points 1 are taken at a small distance h_0 of the invariant curve 0 inside the linear approximation of the invariant curve. Point 2 in I is the image of point 1 in II under Q^1 and Point 2 in II is the image of point 1 in I under Q^0. The manifold is approximated by the straight line joining 1 and 2. The remaining points (from 3 to 5) are obtained in an analogous way. To produce a finer mesh on the manifold, we take a mesh of points in the lines joining 1 and 2 inside sections I and II, and sending this mesh using $Q^{0,1}$ we find a mesh between points 2 and 3, and so on.

The computation of stable manifolds follows the same procedure as before, but using the inverse of the maps P^j (the stable manifold becomes unstable by the inverse map). Note that the inverse maps are easy to obtain since they are the result of integrating backward in time.

4 Results

Let us now present a number of figures showing slices of the stable and unstable manifolds for some tori around L_1 and L_2. All the figures presented here lie in Σ_π.

In Figures 7 and 8, the subfigures (a) and (b) are composed by the curves coming from $\Sigma_{\frac{3\pi}{2}}$ for the stable manifold and from $\Sigma_{\frac{\pi}{2}}$ for the unstable one; the subfigures (c) and (d) are composed, in addition to the previous ones, by the curves coming from Σ_0 for both the stable and the unstable manifolds; and finally, the subfigures (e) and (f) are composed, in addition to the previous ones, by the curves coming from $\Sigma_{\frac{\pi}{2}}$ for the stable manifold and from $\Sigma_{\frac{3\pi}{2}}$ for the unstable one together with the ones coming from Σ_π for both the stable and the unstable manifolds.

Let us explain the last paragraph using other words. We start with an example and generalised it later. Consider Figure 7(a). It is obtained integrating a mesh of points on a fundamental cylinder approximating both the stable and the unstable manifolds of T^{L_2} lying in the section Σ_{f_3}, i.e., it is obtained by applying $(P^3)^{-1}$ and P^1 to the mesh on the fundamental cylinder approximating the stable and the unstable manifolds, respectively. Figures 7(b), 8(a) and 8(b) are obtained the same way. For Figures 7(c), 7(d), 8(c) and 8(d) we apply, in addition to $(P^3)^{-1} : \Sigma_{f_3} \to \Sigma_{f_2}$ and $P^1 : \Sigma_{f_1} \to \Sigma_{f_2}$,

$$(P^3)^{-1} \circ (P^0)^{-1} : \Sigma_{f_0} \to \Sigma_{f_2} \text{ and } P^1 \circ P^0 : \Sigma_{f_0} \to \Sigma_{f_2},$$

i.e., both are integrated a time π departing from the section Σ_{f_0}, backwards for the points close to the stable manifold and forward for the ones close to the unstable one.

As for Figures 7(e), 7(f), 8(e) and 8(f) the only difference is that we apply the ones before and

$$(P^3)^{-1} \circ (P^0)^{-1} \circ (P^1)^{-1} : \Sigma_{f_1} \to \Sigma_{f_2} \text{ and } P^1 \circ P^0 \circ P^3 : \Sigma_{f_3} \to \Sigma_{f_2}$$

together with

$$(P^3)^{-1} \circ (P^0)^{-1} \circ (P^1)^{-1} \circ (P^2)^{-1} : \Sigma_{f_2} \to \Sigma_{f_2} \text{ and } P^1 \circ P^0 \circ P^3 \circ P^2 : \Sigma_{f_2} \to \Sigma_{f_2},$$

all of them, for the points close to the stable and the unstable manifold, respectively.

We have followed a similar strategy as [Jor01]: Each torus is represented by an invariant curve in each temporal section, hence an approximation to the, say, unstable manifold is given by a

shift in the unstable direction of this circle representing the torus. In the application covered in [Jor01] this shifted circle is iterated by the flow and, as the dynamics is not as unstable as the one in the context of $L_{1,2}$ in the PERTBP, these iterations produce a good visualisation for the manifold. In the case of a highly-unstable environment, we use the fundamental cylinder for this visualisation and integrate for less time, more points. More specifically, to produce Figures 7, 8 and 9, the interpolation parameter τ is discritized to produce different "circles" (the parameter θ is also discrtized) which will act as an approximation of the manifold in the given direction.

Although the tori are presented in Figures 7, 8, 9 in pairs, this is not mandatory, as it is not true that they are related one-to-one, like in the PCRTBP. In other words, $T_0^{L_1}$ for instance, may have some influence in (and/or be influenced by) $T_0^{L_2}$, but not only this one, as other ones with closer values of ω. In fact, this is exactly what is used to compute a chain for the Arnold diffusion in the case of the PERTBP [CD23].

In Figure 7 we can see how the stable and the unstable manifolds of the considered tori expand in all directions, while in Figure 8 we consider only the expansion in the direction of Jupiter, in order to better visualise the folds it has in that region.

For Figure 9 the manifolds presented are the ones of $T_0^{L_1}$ and $T_0^{L_2}$. They are analogous to Figures 7(e), 7(f), 8(e) and 8(f), i.e., they present points which were integrated for a time $\pi/2$, π, $3\pi/2$ and 2π coming from Σ_{f_1}, Σ_{f_0}, Σ_{f_3} and Σ_{f_2} (Σ_{f_3}, Σ_{f_0}, Σ_{f_1} and Σ_{f_2}) close to the unstable (stable) manifold, with the difference that the only directions presented are the "opposite-to-Jupiter" ones. The curves presented in red represent a slice of the manifolds that originally go to Jupiter direction. This serves as an illustration of the phenomenon that there are some parts of these manifolds that transit between regions, even considering small time integrations such as 2π, which were not the case for the tori in Figures 7. This is not an statement that they could never experience these type of transition, instead it is a comparison between different behaviours with the same integration times. Moreover, these slices transit between regions (going from Jupiter region from the opposite) guided precisely by the parts of these manifolds that initially grow in these opposite directions, illustrating the phenomenon that they act as guides for the dynamics.

5 Conclusions

In this work, we have shown how to use the multiple shooting technique to compute invariant tori in a highly unstable environment, to analize the linear dynamics around them, and to compute their stable and unstable invariant manifolds.

The computation of invariant tori is done by defining four sections in the phase space and a map from each section to the next, with the goal of computing the four sections of a 2D torus of the flow with these sections. Therefore, we compute the four invariant curves given by these sections.

In addition, for the computation of the linear stability of the computed tori, we have shown how to adapt the computation of the eigenvalues and eigenvectors done to study the stability of invariant curves of maps to this multiple shooting environtment.

Finally, it was also shown how to use the concept of fundamental domain in order to have a better visualization of the manifolds of the computed tori, and how the use of this concept together with the multiple shooting technique lead to improved results.

We have also used continuation methods to obtain the families of tori near $L_{1,2}$ in the suitable range to describe the dynamics of comet 39P/Oterma so that these calculations are used in following papers ([DJ23a, CD23]) to study this transition by showing how these tori and their invariant

manifolds provide an accurate description of the trajectory of the comet from an orbit outside that of Jupiter to a inner one and vice versa, and to produce an initial guess for a diffusion orbit in this model.

References

[CD23] M.J. Capiński and G. Duarte. Computation of a chain for fast Arnold diffusion in the Sun-Jupiter system. Preprint, 2023.

[CDMR06] E. Canalias, A. Delshams, J.J. Masdemont, and P. Roldán. The scattering map in the planar restricted three body problem. *Celest. Mech. Dyn. Astron.*, 95(1-4):155–171, 2006.

[CJ00] E. Castellà and À. Jorba. On the vertical families of two-dimensional tori near the triangular points of the Bicircular problem. *Celest. Mech. Dyn. Astron.*, 76(1):35–54, 2000.

[CM06] E. Canalias and J.J. Masdemont. Homoclinic and heteroclinic transfer trajectories between planar Lyapunov orbits in the Sun-Earth and Earth-Moon systems. *Discrete Contin. Dyn. Syst.*, 14(2):261–279, 2006.

[DJ23a] G. Duarte and À. Jorba. Invariant manifolds of tori near L_1 and L_2 in the Planar Elliptic Restricted Three-Body Problem II. The dynamics of comet Oterma. Preprint, 2023.

[DJ23b] G. Duarte and À. Jorba. Using normal forms to study Oterma's transition in the planar RTBP. *Discrete Contin. Dyn. Syst. Ser. B*, 28:230–244, 2023.

[GJ04] F. Gabern and À. Jorba. Generalizing the Restricted Three-Body Problem. The Bianular and Tricircular Coherent Problems. *Astron. Astrophys.*, 420:751–762, 2004.

[GJNO22] J. Gimeno, À. Jorba, B. Nicolás, and E. Olmedo. Numerical computation of high-order expansions of invariant manifolds of high-dimensional tori. *SIAM J. Appl. Dyn. Syst.*, 21(3):1832–1861, 2022.

[GKL$^+$04] G. Gómez, W.S. Koon, M.W. Lo, J.E. Marsden, J. Masdemont, and S.D. Ross. Connecting orbits and invariant manifolds in the spatial restricted three-body problem. *Nonlinearity*, 17(5):1571–1606, 2004.

[GM01] G. Gómez and J.M. Mondelo. The dynamics around the collinear equilibrium points of the RTBP. *Phys. D*, 157(4):283–321, 2001.

[HB98] N.W. Harris and M.E. Bailey. Dynamical evolution of cometary asteroids. *Mon. Not. R. Astron. Soc.*, 297(4):1227–1236, 07 1998.

[Jor01] À. Jorba. Numerical computation of the normal behaviour of invariant curves of n-dimensional maps. *Nonlinearity*, 14(5):943–976, 2001.

[JV97a] À. Jorba and J. Villanueva. On the normal behaviour of partially elliptic lower dimensional tori of Hamiltonian systems. *Nonlinearity*, 10:783–822, 1997.

[JV97b] À. Jorba and J. Villanueva. On the persistence of lower dimensional invariant tori under quasi-periodic perturbations. *J. Nonlinear Sci.*, 7:427–473, 1997.

[JZ05] À. Jorba and M. Zou. A software package for the numerical integration of ODEs by means of high-order Taylor methods. *Exp. Math.*, 14(1):99–117, 2005.

[KLMR00] W.S. Koon, M.W. Lo, J.E. Marsden, and S.D. Ross. Heteroclinic connections between periodic orbits and resonance transitions in celestial mechanics. *Chaos*, 10(2):427–469, 2000.

[KLMR01] W.S. Koon, M.W. Lo, J.E. Marsden, and S.D. Ross. Resonance and capture of Jupiter comets. *Celest. Mech. Dyn. Astron.*, 81(1-2):27–38, 2001.

[MO17] K.R. Meyer and D. Offin. *Introduction to Hamiltonian dynamical systems and the N-body problem*, volume 90 of *Applied Mathematical Sciences*. Springer, New York, third edition, 2017.

[SB02] J. Stoer and R. Bulirsch. *Introduction to numerical analysis*, volume 12 of *Texts in Applied Mathematics*. Springer-Verlag, New York, third edition, 2002.

[Sim90] C. Simó. On the analytical and numerical approximation of invariant manifolds. In D. Benest and C. Froeschlé, editors, *Modern methods in celestial mechanics*, pages 285–330. Ed. Frontières, 1990. Reprinted at `http://www.maia.ub.es/dsg/2004/index.html`.

[Sze67] V. Szebehely. *Theory of Orbits*. Academic Press, 1967.

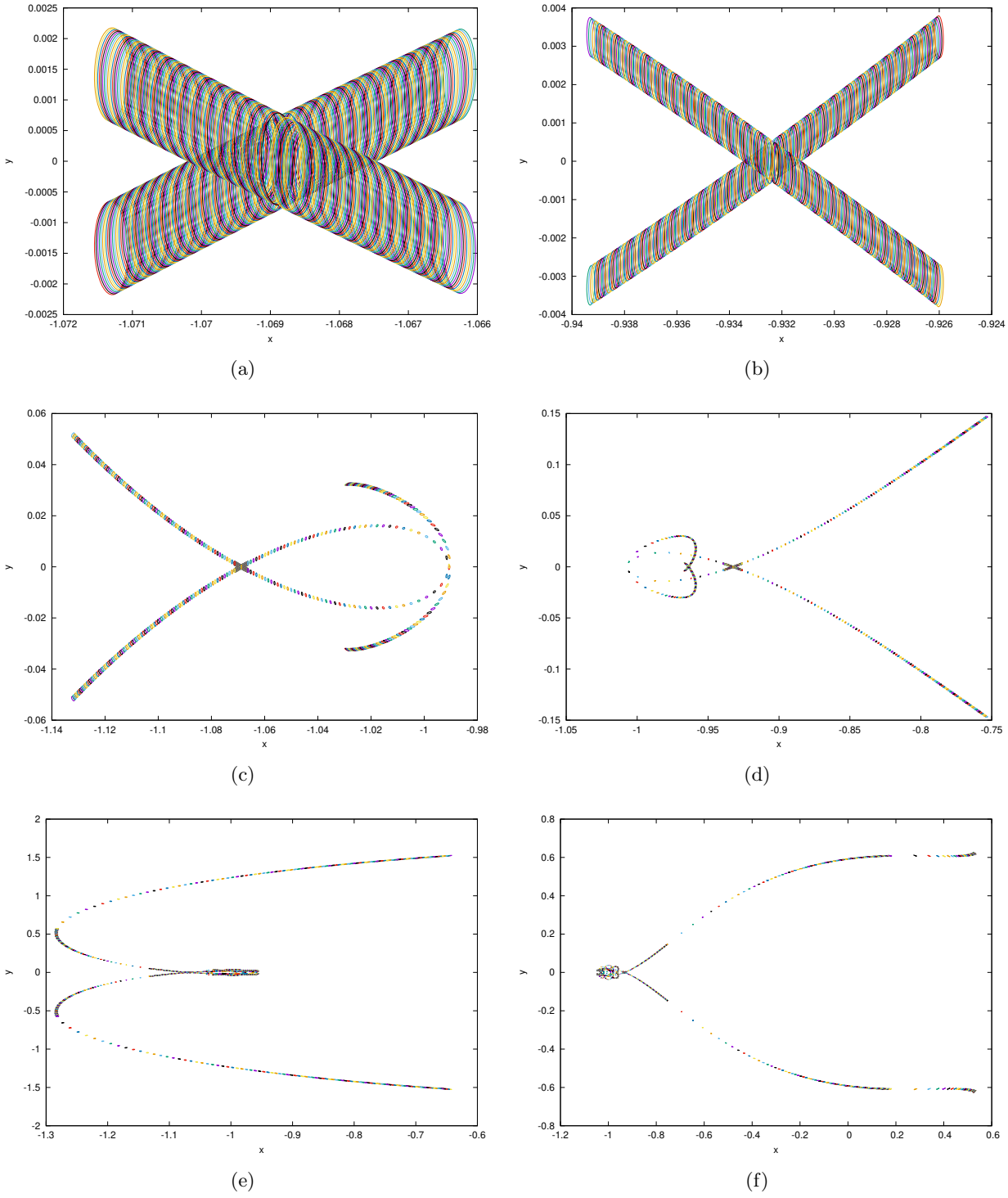

Figure 7: Slices of manifolds of the tori $T^{L_2}_{-1330}$ (left column) and $T^{L_1}_{-2565}$ (right column).

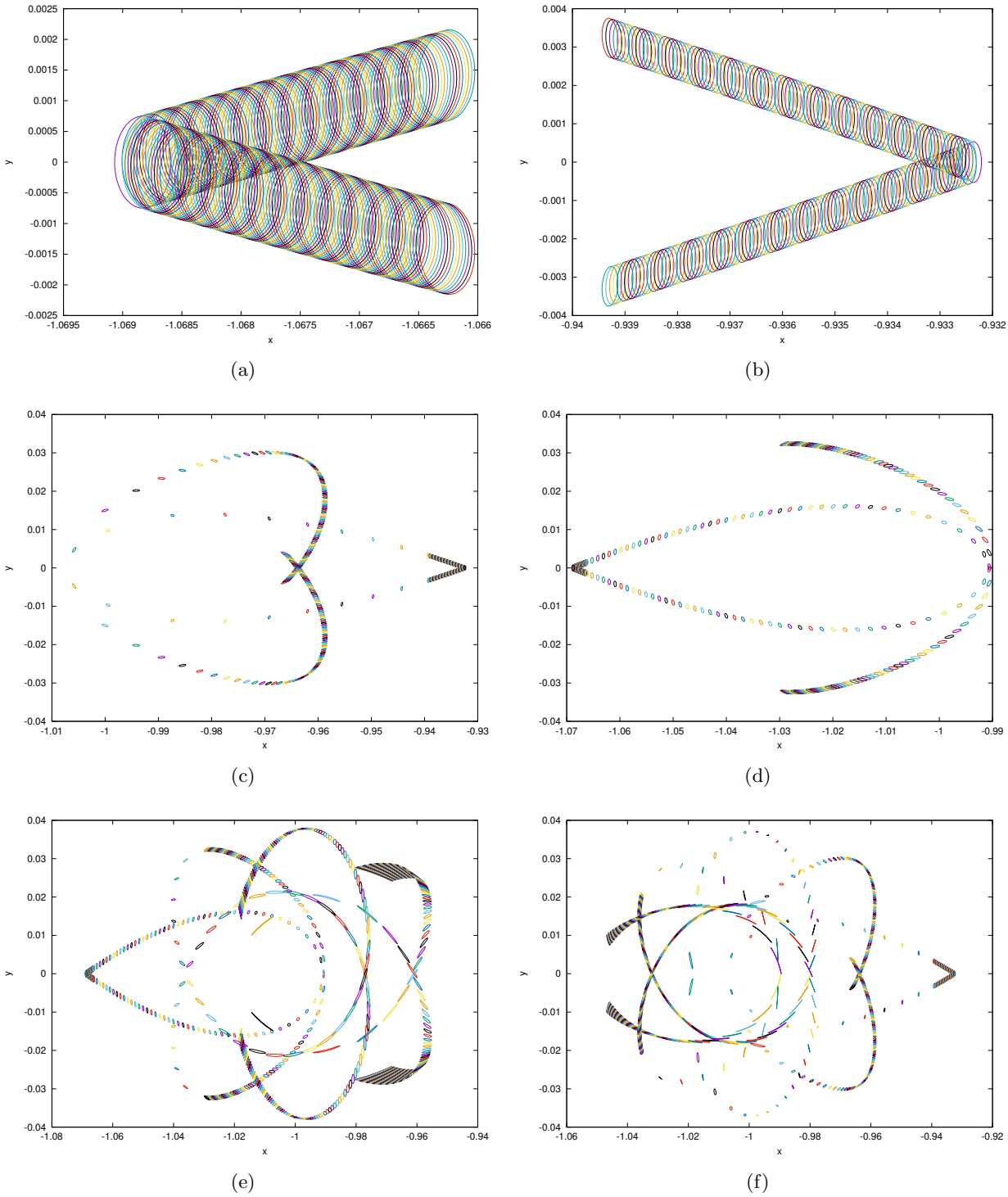

Figure 8: Slices of manifolds of the tori $T^{L_2}_{-1330}$ (left column) and $T^{L_1}_{-2565}$ (right column) in the region around Jupiter.

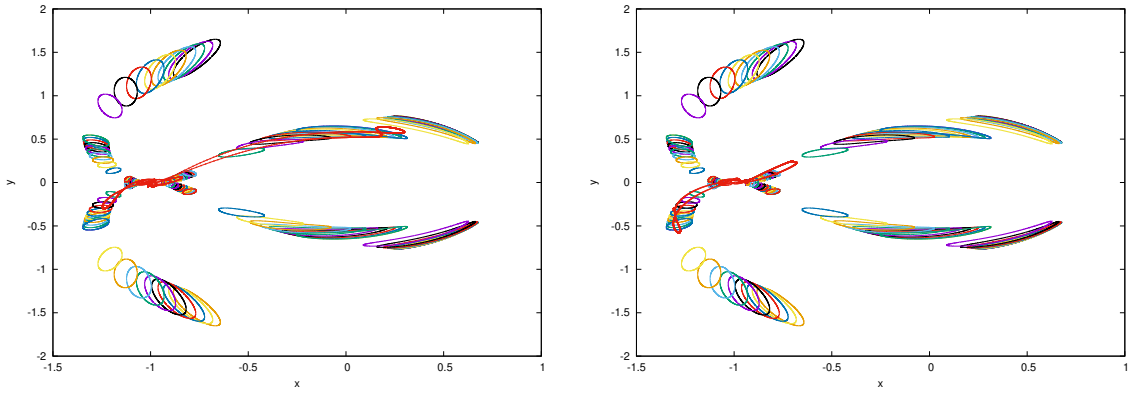

(a) (b)

Figure 9: Slices of the manifolds of $T_0^{L_1}$ and $T_0^{L_2}$ (opposite-to-Jupiter direction) together with some slices in the direction of Jupiter (in red with interpolated points). On the left side, slices of the stable manifold of $T_0^{L_1}$ and, on the right side, the stable manifold of $T_0^{L_2}$.